High-resolution attribution of the daily exposure of people and ecosystems to climate-driven heat

Manuscript submitted to the *Proceedings of the National Academy of Sciences* on November 30, 2023

Andrew J. Pershing[1]*, Kristie L. Ebi[2], Daniel M. Gilford[1], Joseph Giguere[1], Bernadette Woods Placky[1], Benjamin H. Strauss[1]

[1]Climate Central, Inc. Princeton, NJ 08648, USA

[2]Center for Health and the Global Environment, University of Washington, Seattle, WA 98195, USA

*Andrew J. Pershing

Email: apershing@climatecentral.org

Author Contributions: Designed Research: AJP, BWP, BHS, KLE; Performed Research: AJP, DMG, JG; Analyzed Data: AJP, DMG, JG; Wrote Paper: AJP, DMG, KLE, BHS

Competing Interest Statement: Authors declare that they have no competing interests.

Classification: Physical Sciences/Sustainability Science, Social Sciences/Sustainability Science

Keywords: climate change, climate impacts, attribution

Abstract

Climate attribution assessments are now common for exceptional weather events, but lesser extremes and everyday weather remain largely unexamined. Here we use a multi-method approach to calculate the influence of human-caused climate change on 54 years of daily temperatures around the world. We use a new metric called the change in information due to perspective that contrasts the likelihood of a temperature in two climates: one forced by extra greenhouse gases and another with no anthropogenic warming. We show that exposure to climate change surged in the middle of 2023. On August 21, a record 4.9 billion people experienced temperatures made at least twice as likely by climate change. On August 22, 49.5% of the land surface reached this level. The distribution of exposure of both ecosystems and countries in August was largely consistent with long-term trends, with higher exposure at night, in tropical ecosystems, and in less developed countries. Notable exceptions to this pattern occurred in Europe and the United States. On August 21, Spain and Italy experienced anomalously warm conditions with very strong climate fingerprints. Over the second half of the year, cities in the United States from Texas to Florida experienced exceptional streaks of extreme and attributable temperatures. We extend the daily attribution approach to quantify how climate change is increasing the exposure of people, especially in Africa and small island states, to stressfully warm temperatures. Daily climate change attribution of temperature provides a new index of climate exposure and new opportunities to communicate about climate change.

Significance Statement

We quantify the climate fingerprint on local temperature, everywhere and for every day from 1970-2023. We show how the exposure of people and ecosystems to elevated daily temperatures that have been made more likely by climate change surged in 2023. This exposure is not even: it occurs more intensely at night and falls more heavily on countries and ecosystems near the equator. Elevated temperatures are a health risk, and we show that climate change is increasing the exposure of people to stressful daily temperatures. Quantifying climate change on a daily, local scale highlights conditions that will benefit from

adaptation, emphasizes the benefits from reducing carbon emissions, and offers new opportunities to raise public understanding of climate change.

Main Text

Introduction

Rising temperatures have been apparent at the global scale for nearly 40 years (1), and attributable to humans for more than two decades (2). Global temperatures increased rapidly in the middle of 2023. July was the warmest month ever measured (3), September had the maximum temperature anomaly (4), and November 2022-October 2023 was the warmest 12 month period (5).

While the global statistics are important for tracking climate change, people and ecosystems experience climate change through changes in daily weather. Our ability to detect climate change at finer spatial and temporal scales has increased. This is most apparent in the advent of extreme event attribution (6, 7), which has been used to diagnose the contribution of climate change to individual heatwaves (8), extreme rainfall events (9, 10), and economic damages from coastal flooding (11).

Gilford et al. (12) (hereafter G22), extended extreme event attribution methods (i. e. 6, 7), to daily temperatures and demonstrated the ability to quantify how climate change has made a wide range of temperatures, not merely extremes, more likely. This daily, local scale perspective provides new capabilities to consider how people and ecosystems around the world experience climate change.

We apply the G22 approach, which blends observed trends and climate models, to quantify the likelihood of the observed temperatures (daily minimum, maximum, and average) during the record warm conditions of 2023. We use a new metric called the change in information due to perspective (ChIP) to contrast the likelihoods to those in a counterfactual world with no global warming, and we extend the calculations back 54 years to place the conditions in 2023 in the context of long-term trends.

Measuring Climate Change through Information

Climate change attribution studies are built around a contrast between our current world and a counterfactual world with similar population distribution but no anthropogenic warming (13). Most studies quantify the influence of climate change on the event using the ratio of the probability an event of similar or greater magnitude in the current climate to the probability in the counterfactual climate (6). This approach is suitable for quantifying specific, high-impact events, but a metric built around the probability of exceedance is less informative for events that are more common.

For this study, we use the relative log-likelihood, i.e. the log of the ratio of the value of the probability density function of the event in the current climate to the value in the counterfactual climate. Focusing on the relative likelihood of an event, rather than the probability of exceedance, allows us to apply this metric to any temperature, not just extremes. For example, a cool temperature that is less likely in the current climate will have a negative value. The logarithmic formation makes sums and averages meaningful, allowing us to aggregate over space and time.

We refer to the metric as the change in information due to perspective (ChIP) to highlight the connection with information theory (see Supplement for more details). Information theory centers the notion of an observer. The observer has expectations about events that are quantified as a probability distribution. New events give the observer access to new information, and the amount of information available is proportional to how novel or surprising the event is. For an observer from the modern climate, ChIP is the information advantage they have due to their understanding of climate change.

Results

We used G22's multi-method approach to calculate temperature distributions in the counterfactual climate (0°C of warming relative to the 1850-1900 average) and the modern climate based on the warming observed in the specified year. We then used these distributions to calculate the ChIP for daily high (Tmax), low (Tmin), and average (Tavg) temperatures over land from the ERA5 reanalysis for every day from January 1970-October 2023 at 0.25° spatial resolution (see Methods).

As global temperatures increased in 2023, so did the exposure to daily temperatures fueled by human-caused climate change. We anchor our analysis on August 22, which is the day when the global average ChIP reached its maximum observed level. On that date, very high ChIP levels were observed across most of Africa and Europe and extended from Brazil to the United States (Figure 1A). In Asia, the Arabian Peninsula, India, southeast Asia, and the Malay Archipelago were also at very high levels. In aggregate, 49.5% of the land surface experienced conditions where the ChIP was at or above 1, indicating temperatures that were made at least twice as likely because of climate change. In contrast, only 3.3% of the land surface experienced conditions where the ChIP was at or below -1.

ChIP incorporates a range of information including the variance in temperature (captured by the probability distributions) and the expected change in temperature due to climate change. It thus provides new information beyond the temperature anomaly. On average, temperature anomalies are stronger at mid and high latitudes and weaker in the tropics. However, low temperature variability near the equator and consistent warming in both the observations and climate models give a stronger ChIP response at low latitudes. For example, on August 22, 2023, western Africa was only slightly warmer than average (Figure 1A), yet Accra, Ghana had a ChIP of 4.0 (Figure 1B). In contrast, some of the highest temperature anomalies on that date were found in North and South America: despite a temperature anomaly of 10°C, Asunción, Paraguay had a ChIP of 1.8.

Global average ChIP values typically peak at the end of boreal summer (Figure 1C, inset), but the increase in 2023 was unprecedented. From 1970-2022, global average ChIP never exceeded 1.0 (Figure 1C), rarely exceeded 0.8 in the previous three years (Figure 1D), but in 2023, values rose to a peak of 1.26 on August 2023 (Figure 1E).

Area-weighted ChIP time series reveal another notable pattern: local experiences with climate change are typically stronger at night. The annual average ChIP values for Tmin (Figure 1, C-E, black lines) were consistently higher than those for both Tavg (gray) and Tmax (yellow). Tavg is only slightly lower than Tmin, indicating that rising nighttime temperatures are driving the increase in the attribution levels for Tavg.

The distribution of life on the planet reflects the variations in climatic conditions (14), leading to recognizable biomes. Because ChIP incorporates, it quantifies changes that are likely to be ecologically meaningful. On the record exposure day, there was a strong latitudinal gradient in the exposure of terrestrial biomes to climate change (Figure 2A). Four tropical biomes: rainforests, mountain systems, shrublands, and moist forests had area-average ChIP values above 2. This means that on average, the organisms in these systems experienced temperatures that were made at least four times more likely by climate change. Boreal and polar ecosystems had much lower exposure on that date with both low temperature anomalies and low ChIP values.

The annual average exposure of tropical and subtropical ecosystems systems to climate change as measured by ChIP has increased at a rate of 0.18 and 0.07 decade^{-1}, respectively (Figure 2B). In contrast, ChIP values across boreal and polar ecosystems have increased at only 0.04 decade^{-1}. The exposure of all climatic regions increased in 2023 (Figures 2C). With the exception of polar systems, which had higher exposure than boreal systems, the tropical-to-boreal gradient in ChIP on August 22 is consistent with the long-term trends (Figure 2D).

To quantify the exposure of humans to climate change, we calculated the population-weighted (based on the distribution of people in 2020 (15)) average temperature anomalies and ChIP values for the globe and for 175 countries. Based on Tavg, the maximum exposure of humans to climate change occurred on August 21, 2023, the day before the maximum exposure of the land surface. On that date, 4.9 billion people experienced conditions with ChIP ≥1. The elevated human exposure was driven by high ChIP values in India, southeast Asia, western Africa, Europe, and central America.

On the day of maximum human exposure, Rwanda, Burundi, and Guatemala had the highest per-capita ChIP values among 91 countries with more than 10 million residents (Figure 2C). Residents in these countries experienced temperatures with ChIP values that approached 4.0, the maximum value of our current system. According to the human development index (16), these three countries are categorized has having “Low” (Rwanda and Burundi) and “Medium” (Guatemala) development levels.

Overall, poorer, less-developed countries had higher exposure on August 21 than wealthier, more developed countries. There were 18 countries with per-capita average ChIP values above 3. Of these countries, 15 are either in the “Low” (9 countries) or “Medium” (6 countries) categories. On the other end of the exposure spectrum, there were 11 countries with average ChIP values below 1, and all but three countries: Kyrgyzstan (“Medium), China (“High”), and Algeria (“High) are classified as very highly developed. Japan, and many countries in Europe ran counter to this pattern. They had relatively high (ChIP>2) exposure to climate change, and several such as Spain and Italy had very high exposure and large anomalies..

The relationship between development level and exposure in August 2023 is consistent with the long-term patterns. Per-capita exposure in the “Low” development category has risen at a rate of 0.20 ChIP decade^{-1} (Figure 2F), a rate that is faster than tropical ecosystems. Countries in the “Very High” category have experienced a more gradual increase of 0.07 ChIP decade^{-1}. The relative ordering of development types on August 21 (Figure 2H) was broadly consistent with the long term trends. The exception was that hot conditions in Europe and Japan pushed the “Very High” category above the “High” category on that day.

Rising temperatures pose a considerable health risk, and our methods allow us to estimate how increased exposure to climate-driven heat has intensified these risks. We define the minimum mortality temperature as the 83rd percentile of daily Tavg over the period 1986-2005 (16, 17). As temperatures rise above this level, mortality increases. Because the minimum mortality temperature is defined relative to a percentile rather than an absolute temperature, this temperature is location-specific, with lower values at higher latitudes and elevations (Figure S2).

In the absence of a warming trend, we would expect 62 days per year (17% of 365) above the minimum mortality temperature. Instead, we find that the population-weighted average number of days above the minimum mortality temperature (Figure 3A orange) has been above 62 every year since 2002. The population exposure to cold conditions (below the 17th percentile) was nearly the same as the exposure to high temperatures at the beginning of the time series (Figure 3A gray). While exposure to stressfully cold temperatures decreased at a rate of 0.6 days yr^{-1}, per capita exposure to stressfully warm days increased twice as fast (1.3 days).

Over the period 2018-2023, more than half of the high temperature days also had ChIP ≥1 (Figure 3A black). This indicates that climate change is amplifying human exposure to dangerous heat by increasing the number of days about the minimum mortality threshold. The number of days with both stressful temperatures and elevated ChIP increased most strongly in small island nations and Africa and less strongly in Oceania and Europe (Figure 3A thin lines). For days that would have been above the threshold even in the counterfactual climate, the elevated ChIP values indicate temperatures that are warmer and therefore more dangerous.

In 2023, most locations experienced more than 62 days above the minimum mortality temperature (Figure 3B, area-weighted average = 87.2 days), and nearly the entire land surface had some days above this threshold and with ChIP ≥1 (Figure 4C, area-weighted average = 52.9 days). Many locations, especially near the equator, had 70 or more days with ChIP ≥1, indicating that the climate change at least doubled the risk of broad, daily exposure during nearly 1 in 5 days of 2023. Whether mortality is actually observed to increase depends on a wide range of factors in addition to exposure to high temperatures, including access to healthcare, the proportion of the population at higher risk because of underlying susceptibilities, the presence of an early warning system, and urban form (18).

Even in an unaltered climate, temperatures above the minimum mortality temperature will be relatively common. To consider exposure to even more extreme temperatures, we calculated the location-specific 99th percentile temperature. For 700 cities with more than 1 million residents, we looked for periods of more than five consecutive days (termed streaks) during the last year (see Table S3). The United States had 7 cities on the list of cities with the top 20 longest streaks (Table 1), and the 22 day streak in Houston, Texas was the longest observed. Other cities from G20 nations with significant streaks included Mexico (3), Indonesia (4), Brazil (1), China (1), and India (1).

The average daily ChIP for each of these streaks underestimates the impact of climate change on these events. The ChIP for an n-day average temperature can be calculated by scaling the n-day average ChIP

by the ratio of the variance of multiway averages to the variance of daily averages (see Supplement). Applying this formula, the 10-day streak in Miami, Florida, United States had the highest climate change exposure, with a multi-day ChIP of 7.3.

Discussion

Global temperatures are warmer than they have been in 125 thousand years (19), and the 12 month period from November 2022-October 2023 was the hottest ever measured. Daily attribution objectively quantifies the influence of climate change on local temperatures, connecting the experience of people and ecosystems to global warming.

The exposure of ecosystems on August 22, 2023 was highly consistent with the long-term trend, supporting Sippel et al.'s (20) conclusion that the spatial fingerprint of climate change is detectable in distribution of daily weather conditions. A major feature of this global pattern is elevated exposure in the tropics. In these regions, the relatively low day-to-day variability in conditions makes the signal of climate change much clearer, even when average anomalies are lower than at higher latitudes (21). The stronger tropical fingerprint of climate change increases the ecosystem exposure to previously atypical and likely stressful conditions, with potentially detrimental results. This elevated exposure is particularly acute for ecosystems like tropical rainforests that are hot spots of biodiversity and carbon (22, 23), and the spatial pattern is consistent with projections of future impacts to these ecosystems (24).

The latitudinal gradient in exposure to climate change also means that people in Africa and Central America have higher exposure than people in higher latitude countries like the United States and China. Although it is too soon to say whether this is part of a trend, many wealthy countries were hit with very unusual conditions in 2023. For example, the population-weighted average ChIP in the United States on August 21 was relatively low, yet cities in the southern United States were exposed to many days of extreme and attributable heat. The interaction between attributable warming, urban heat island effects, and population growth can lead to especially strong exposure in cities (25, 26).

Our results show that human-caused climate change is having a quantifiably stronger impact on Tmin. Davy et al. (27) note that nighttime temperatures are expected to warm rapidly in response to rising greenhouse gases, and faster warming at night has been observed since the early 1990s (28). The consequences of rising nighttime temperatures have received relatively little mention in the ecological literature (29) compared with agricultural studies that link elevated nighttime temperatures with reduced yields and altered nutritional properties in commercial crops such as wheat and rice (30, 31). Warmer conditions at night make it harder for people to recover from the heat of the day, increasing health risks (32).

Rising temperatures pose a growing health risk (18). The notion of a location-specific minimum mortality temperature emerges from the ability of people to adapt to prevailing conditions, through a combination of physiological acclimatization and behavioral and technological adaptation (33). Future health impacts from exposure to high temperatures are sensitive to projected adaptation rates (34). There is some evidence that adaptation is occurring, especially in high income countries (18, 35). The fact that low-income countries are experiencing more days with detectable climate fingerprints they are facing increasingly greater risks and adaptation challenges. Daily attribution, especially when connected with impacts on health or economies, could support efforts by developing countries to gain compensation for losses and damages from climate change (36).

By framing climate change attribution as an information problem, ChIP measures the information advantage of an observer knowledgeable about climate trends. This advantage is not shared by natural systems and even many human systems that adapt through backward-facing processes. These systems embed knowledge of past conditions, and conditions outside of the past experience—surprises— can lead to losses in functionality (37). Repeated and widespread high ChIP values thus are likely to reflect conditions that are stressful to these systems, and we hypothesize that ChIP should be a good indicator of the intensity of local climate impacts and could be used to inform adaptation priorities.

Daily climate change attribution can also play a crucial role expanding public understanding of climate change. Frequent communication about climate change in the context of weather broadcasts has been shown to lead to a greater interest in addressing climate change (38). Because the ChIP metric can be

applied to any temperature, including forecasted temperatures, it could be incorporated into regular discussions of the weather. The daily attribution approach also allows us to detect events in places or seasons that may not garner as much public attention, and can help address the lack of attribution studies in the developing world (39).

Materials and Methods

This study uses three main kinds of data: global mean temperature, localized daily temperatures, and the distribution of people across the globe:

Global Mean Temperature: HadCRUT5

Global mean temperature is used to understand how local temperatures change in response to global warming. We used the UK Met Office Hadley Centre/Climatic Research Unit Temperature data set, version 5 (HadCRUT5)(40). We subtracted the mean of the period 1850 to1899 from the yearly data. This allows us to work in temperature change relative to pre-industrial period, consistent with temperature changes used by the IPCC.

Daily Temperatures: ERA5

We used 2m air-temperature from the ERA5 reanalysis (41). We downloaded hourly data in 3-hour intervals for the period 1950-2022. For each day (defined relative to UTC), we computed the minimum (Tmin) and maximum (Tmax) over that period. We then calculated the daily average (Tavg) as the average of Tmin and Tmax.

Population Data: GPWv4

We used the Gridded Population of the World Version 4 (GPWv4, revision 11) data on the distribution of people in 2020, adjusted to the UN World Population Program values (15). We used the xESMF (42) bilinear interpolator to regrid the GPWv4 data to the 0.25° ERA5 grid.

Daily Attribution Methodology

Our daily attribution system is based on G22's multi-method approach (12). This approach uses two empirical methods to estimate the frequency of temperatures in the modern climate and a counterfactual climate with no anthropogenic warming. It also uses paired climate models run with and without greenhouse gas forcing. We summarize these methods below. More details are available in the Supplement Materials.

Calculating the ChIP for an observed temperature (T) requires estimating the likelihood of T in the climate in which it was observed (which we refer to as "modern") and in the counterfactual climate with no global warming. We define the modern climate based on the smoothed global mean temperature in the year when T occurred (GMT_{yr}). The two climates are represented by skew normal distributions. This means that ChIP is

$$\mathrm{ChIP}(T) = -\log_2(SN_0(T)) + \log_2(SN_{yr}(T)) \quad (3)$$

where SN_0 and SN_{yr} are the distributions representing the counterfactual and modern climates.

G22 uses multiple approaches to estimate the modern and counterfactual climates. The most straightforward method uses paired climate models provide a direct estimate of the influence of anthropogenic greenhouse gas emissions on local conditions. We used 24 models from CMIP6 that had historical runs, forced projections (SSP3-7.0 if available, SSP5-8.5 in some cases), and pre-industrial control runs (Table S2). The modern climate is created by fitting the skew normal distribution to the data within a seasonal period of 31 days across 31 years centered on the year when the model's GMT first exceeded GMT_{yr}. The counterfactual climate is the constructed from the same seasonal period in the pre-industrial control run. The model outputs were bias-corrected based to the ERA5 data from 1991-2020 using (43). All models were regridded using (42) to a common 1.5°-by-1.5° grid. We use 24 seasonal periods centered on the 1st and 15th of each month.

G22 also outlined two empirical approaches. Both rely on establishing *B*, the expected change in local temperature in response to a 1° change in GMT. We use linear regression over the period 1950-2022 to estimate B_q for 21 evenly-spaced temperature quantiles (q) between 0.01 and 0.99. The first empirical

method assumes that warming uniformly affects all parts of the distribution. For this method, we fit a skew normal distribution to data from the seasonal period across the 1991-2020 reference period. We then shift the location of the distribution by $B_{0.5}$*(GMT_{yr}-GMT_{2005}) to create the modern distribution. The counterfactual distribution is created by applying a shift of $B_{0.5}$*(0 - GMT_{2005}).

G22's quantile method allows the shape of the distribution to change. To compute the modern distribution, we bin the reference data by the quantiles, shift each bin by B_q*(GMT(yr)-GMTref), and then fit the skew normal distribution. The counterfactual distribution is computed analogously using a shift of B_q*(0 - GMT_{2005}).

Once the distributions are computed, we compute ChIP(T) by applying equation (3) to the 24 pairs of model climates and the two sets of empirical climates. We then create a single estimate of ChIP by averaging the two empirical estimates, averaging the 24 model estimates, and then averaging the two averages.

By definition, most temperatures will fall near the center of the distributions, producing ChIP values near zero. As temperatures move away from the tails, the magnitude of ChIP generally increases but our confidence in the underlying distributions decreases. For this reason, values above 4 or below -4 were replaced with 4 or -4, respectively. This means that the ChIP values used in this study are conservative. They are more reliable for the temperatures commonly encountered but they will underestimate the information advantage for extreme temperatures.

We note that our system is almost entirely self-consistent. Observed temperatures from ERA5 are compared against scale factors and probability distributions derived from ERA5. This approach is resistant to any constant bias that may occur with ERA5.

Trends in ChIP

For the time series depicted in Figures 2-3, we computed the trend in ChIP using linear regression. All trends were significant at $p<0.01$ and had R^2 values above 0.75.

Attributable Temperatures and Human Health

We used the Tavg from ERA5 to define the temperature thresholds for our health analysis. For each location, we calculated the 83rd percentile (MMT_{hot}) and 17th percentile (MMT_{cold}) of the daily temperatures for the period 1986-2005 (Figure S2). This period was used for the the IPCC Fifth Assessment Report and was selected by the Lancet Countdown as their standard reference period (16).

For every day, we flagged local temperatures that were above MMT_{hot}. We then summed the number of these days over each year (i.e. Figure 3A and B). We also multiplied by the GPWv4 population and then summed to get the total exposure of people to high temperatures. We also totaled the number of days that were above the temperature threshold and that also had ChIP(T)≥1. The procedure was repeated using T<MMT_{cold} and ChIP(T)≤-1. These results are displayed in Figure S3.

Acknowledgments

This study would not have been possible without significant technical support from the Climate Central software team. We are particularly grateful to D. Dodson, Z. Belki, and B. Mares for their help with this project. Major funding provided by the Bezos Earth Fund, the Schmidt Family Foundation/Schmidt Futures Fund, High Meadows Foundation and the William and Flora Hewlett Foundation (AJP, DMG, JG, BWP, BHS).

References

1. J. Hansen, S. Lebedeff, Global trends of measured surface air temperature. *Journal of geophysical research: Atmospheres* **92**, 13345-13372 (1987).
2. IPCC (2001) Climate Change 2001: The Scientific Basis. Contribution of Working Group I to the Third Assessment Report of the Intergovernmental Panel on Climate Change. (Cambridge, U.K. and New York, NY U.S.A.), p 881.
3. Copernicus Climate Change Service (2023) July 2023 sees multiple global temperature records broken.

4. Copernicus Climate Change Service (2023) 2023 on track to become the warmest year after record October. in *Monthly Climate Bulletin*.
5. Climate Central (2023) The hottest 12-month stretch in recorded history.
6. F. E. L. Otto, Attribution of weather and climate events. *Annual Review of Environment and Resources* **42**, 627-646 (2017).
7. D. L. Swain, D. Singh, D. Touma, N. S. Diffenbaugh, Attributing Extreme Events to Climate Change: A New Frontier in a Warming World. *One Earth* **2**, 522-527 (2020).
8. P. A. Stott, D. A. Stone, M. R. Allen, Human contribution to the European heatwave of 2003. *Nature* **432**, 610-614 (2004).
9. G. J. Van Oldenborgh *et al.*, Attribution of extreme rainfall from Hurricane Harvey, August 2017. *Environmental Research Letters* **12**, 124009 (2017).
10. K. A. Reed, M. F. Wehner, C. M. Zarzycki, Attribution of 2020 hurricane season extreme rainfall to human-induced climate change. *Nature Communications* **13**, 1905 (2022).
11. B. H. Strauss *et al.*, Economic damages from Hurricane Sandy attributable to sea level rise caused by anthropogenic climate change. *Nature communications* **12**, 2720 (2021).
12. D. M. Gilford, A. J. Pershing, B. H. Strauss, K. Haustein, F. E. L. Otto, A multi-method framework for global real-time climate attribution. *Advances in Statistical Climatology, Meteorology and Oceanography* **8**, 135–154 (2022).
13. S. Philip *et al.*, A protocol for probabilistic extreme event attribution analyses. *Adv. Stat. Clim. Meteorol. Oceanogr.* **6**, 177-203 (2020).
14. J. D. Witman, A. J. Pershing, J. F. Bruno, Smooth and Spiky: The Importance of Variability in Marine Climate Change Ecology. *Annual Review of Ecology, Evolution, and Systematics* **54**, 129-149 (2023).
15. Center for International Earth Science Information Network (CIESIN), Gridded Population of the World, Version 4 (GPWv4): Population Density Adjusted to Match 2015 Revision of UN WPP Country Totals, Revision 10. NASA Socioeconomic Data and Applications Center (SEDAC).
16. M. Romanello *et al.*, The 2023 report of the Lancet Countdown on health and climate change: the imperative for a health-centred response in a world facing irreversible harms. *The Lancet* (2023).
17. A. Tobías *et al.*, Geographical variations of the minimum mortality temperature at a global scale: a multicountry study. *Environmental Epidemiology* **5**, e169 (2021).
18. K. L. Ebi *et al.*, Hot weather and heat extremes: health risks. *The Lancet* **398**, 698-708 (2021).
19. IPCC, *Climate Change 2021: The Physical Science Basis. Contribution of Working Group I to the Sixth Assessment Report of the Intergovernmental Panel on Climate Change*. V. Masson-Delmotte *et al.*, Eds. (Cambridge University Press, Cambridge, United Kingdom and New York, NY, USA, 2021), vol. In Press.
20. S. Sippel, N. Meinshausen, E. M. Fischer, E. Székely, R. Knutti, Climate change now detectable from any single day of weather at global scale. *Nature Climate Change* **10**, 35-41 (2020).
21. C. Mora *et al.*, The projected timing of climate departure from recent variability. *Nature* **502**, 183-187 (2013).
22. S. L. Lewis, D. P. Edwards, D. Galbraith, Increasing human dominance of tropical forests. *Science* **349**, 827-832 (2015).
23. G. Beaugrand, Towards an Understanding of Large-Scale Biodiversity Patterns on Land and in the Sea. *Biology* **12**, 339 (2023).
24. C. H. Trisos, C. Merow, A. L. Pigot, The projected timing of abrupt ecological disruption from climate change. *Nature* **580**, 496-501 (2020).
25. C. Tuholske *et al.*, Global urban population exposure to extreme heat. *Proceedings of the National Academy of Sciences* **118**, e2024792118 (2021).
26. A. M. Vicedo-Cabrera *et al.*, The burden of heat-related mortality attributable to recent human-induced climate change. *Nature climate change* **11**, 492-500 (2021).
27. R. Davy, I. Esau, A. Chernokulsky, S. Outten, S. Zilitinkevich, Diurnal asymmetry to the observed global warming. *International Journal of Climatology* **37**, 79-93 (2017).
28. T. R. Karl *et al.*, A new perspective on recent global warming: asymmetric trends of daily maximum and minimum temperature. *Bulletin of the American Meteorological Society* **74**, 1007-1024 (1993).
29. C. J. Speights, J. P. Harmon, B. T. Barton, Contrasting the potential effects of daytime versus nighttime warming on insects. *Current Opinion in Insect Science* **23**, 1-6 (2017).
30. S. Peng *et al.*, Rice yields decline with higher night temperature from global warming. *Proceedings of the National Academy of Sciences* **101**, 9971-9975 (2004).
31. S. M. Impa *et al.*, High night temperature effects on wheat and rice: Current status and way forward. *Plant, Cell & Environment* **44**, 2049-2065 (2021).

32. P. Murage, S. Hajat, R. S. Kovats, Effect of night-time temperatures on cause and age-specific mortality in London. *Environmental Epidemiology* **1**, e005 (2017).
33. A. Tobías *et al.*, Geographical variations of the minimum mortality temperature at a global scale: a multicountry study. *Environmental epidemiology* **5** (2021).
34. T. Carleton *et al.*, Valuing the global mortality consequences of climate change accounting for adaptation costs and benefits. *The Quarterly Journal of Economics* **137**, 2037-2105 (2022).
35. M. A. Folkerts *et al.*, Long Term Adaptation to Heat Stress: Shifts in the Minimum Mortality Temperature in the Netherlands. *Frontiers in Physiology* **11**, 225 (2020).
36. I. Noy *et al.*, Event attribution is ready to inform loss and damage negotiations. *Nature Climate Change*, 1-3 (2023).
37. A. J. Pershing *et al.*, Challenges to natural and human communities from surprising ocean temperatures. *Proceedings of the National Academy of Sciences of the United States of America* **116**, 18378-18383 (2019).
38. T. A. Myers *et al.*, Impact of the climate matters program on public understanding of climate change. *Weather, Climate, and Society* **12**, 863-876 (2020).
39. F. E. L. Otto *et al.*, Challenges to Understanding Extreme Weather Changes in Lower Income Countries. *Bulletin of the American Meteorological Society* **101**, E1851-E1860 (2020).
40. C. P. Morice *et al.*, An updated assessment of near-surface temperature change from 1850: The HadCRUT5 data set. *Journal of Geophysical Research: Atmospheres* **126**, e2019JD032361 (2021).
41. H. Hersbach *et al.*, ERA5 hourly data on single levels from 1940 to present.
42. J. Zhuang, R. Dussin, A. Jüling, S. Rasp (2020) xESMF: v0.3.0.
43. S. Lange, Trend-preserving bias adjustment and statistical downscaling with ISIMIP3BASD (v1. 0). *Geoscientific Model Development* **12**, 3055-3070 (2019).

Figures and Tables

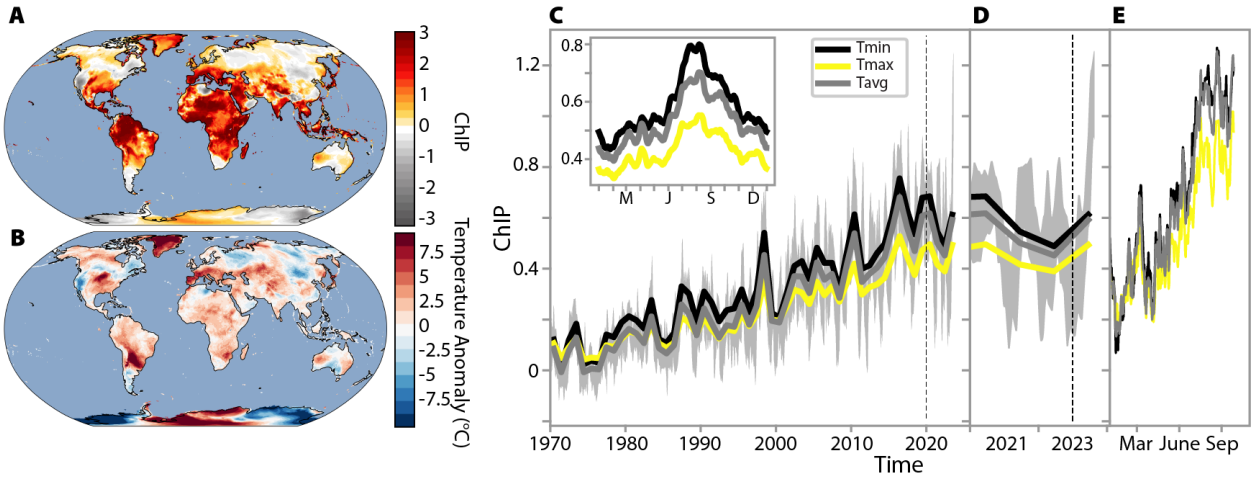

Figure 1. Climate change exposure for 2023. The distribution of ChIP(A) and temperature anomalies (relative to 1991-2020) (B) for Tavg on August 22, 2023. The standard error of ChIP is shown in Figure S4. Time series of Tavg (gray), Tmax (yellow), and Tmin (black) for the entire period (C), 2018-2022 (D), and November 2022-October 2023 (E). The thick lines in C and D are the annual averages of the area-weighted average over the land surface, and the gray shading in C and D shows a representative range of daily Tavg (rolling 45 day minimum and maximum, smoothed by a 30 day running mean). The vertical dashed lines indicate the first time shown in the next panel. The daily data for the last 12 months are shown in E. Inset: ChIP climatology based on the 2018-2022 average and smoothed using a 15 day running mean.

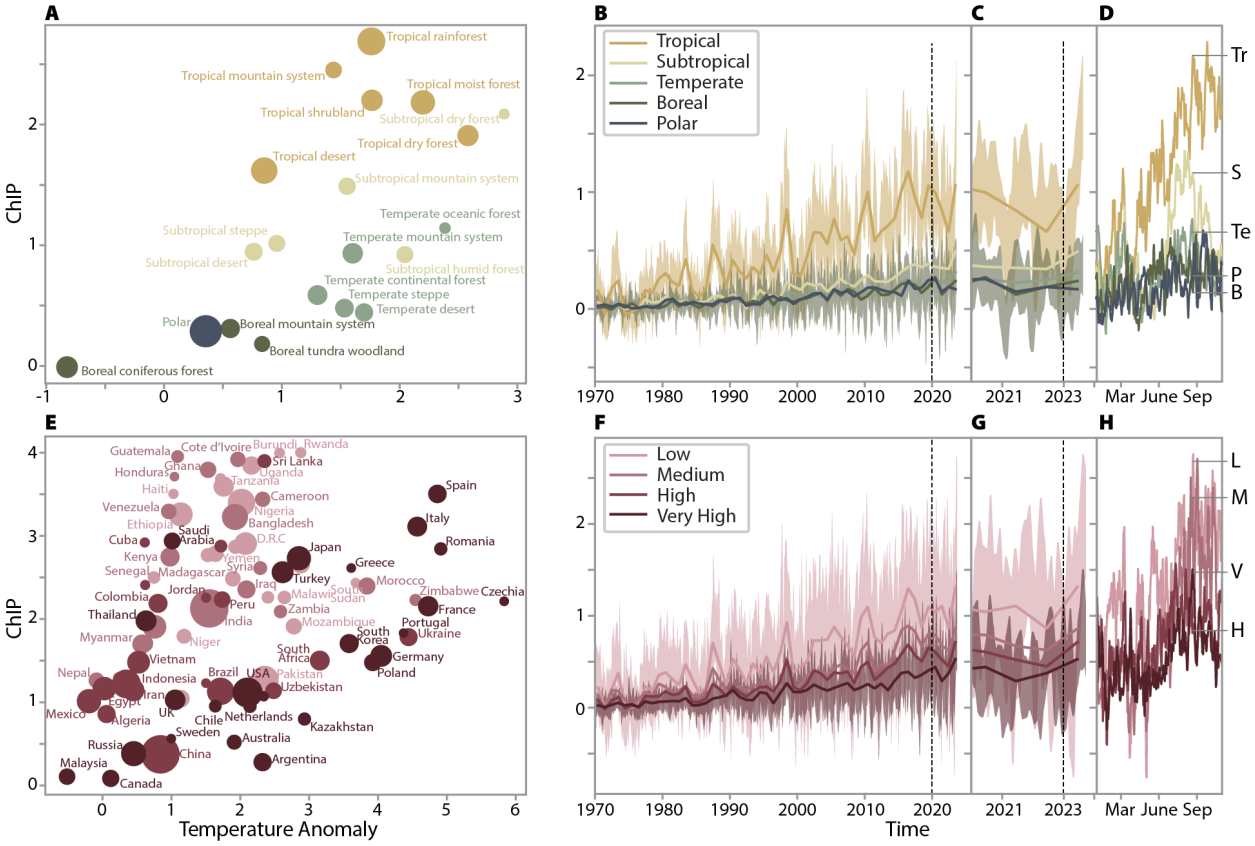

Figure 2. Climate change exposure of biomes and countries. A. Area-weighted average exposure of biomes on August 22 to temperature anomalies (horizontal axis) and ChIP (vertical axis). The size of each circle indicates the relative area of the biome. Color indicates climate zone. B-D. Time series for biomes aggregated by climate zone. The panels display time periods as in Figure 1. E. Population-weighted average exposure for countries with over 10 million people on August 21. Size indicates relative population and color indicates human development index level. F-G. Time series aggregated by human development index. The labels on the right of D and H show the ChIP level reached by each grouping on the maximum exposure day.

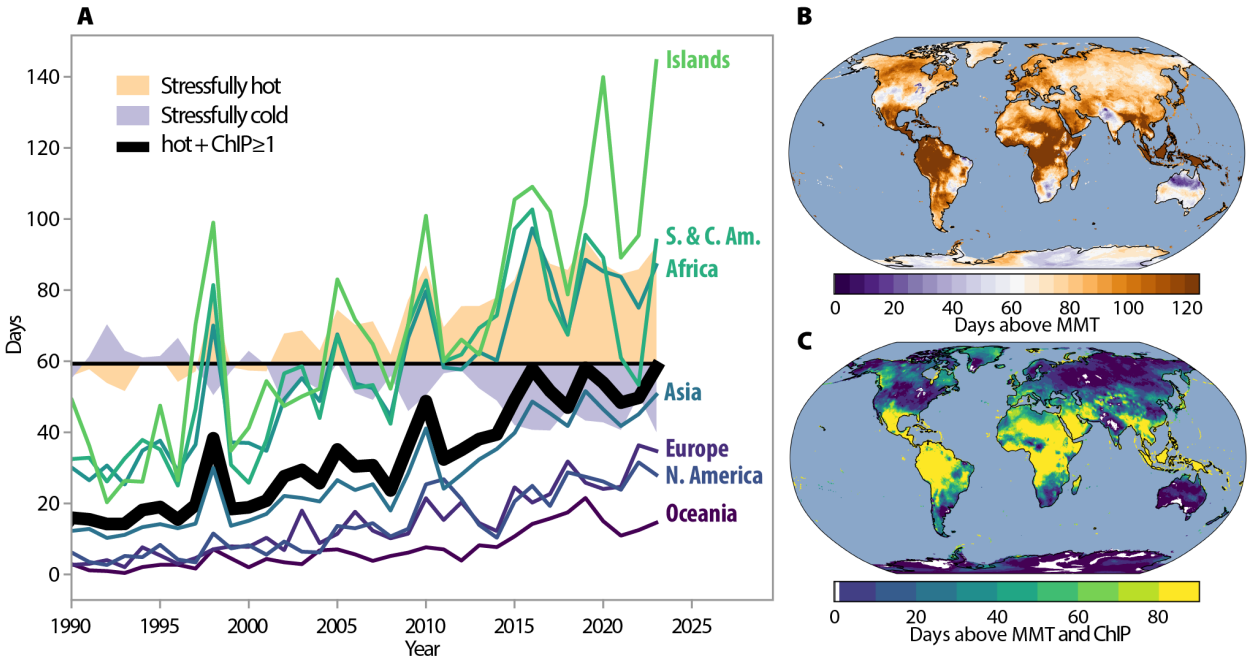

Figure 3. Exposure to stressful temperatures. A. Population-weighted exposure to days above the minimum mortality temperature (MMT) defined by 83rd percentile (orange shading) and days below the 17th percentile (blue shading). Both time series are referenced against 62 days, the number expected in a stable climate. The number of days of exposure to warm temperatures that were made at least twice as likely by climate change (ChIP≥1) is plotted as a solid black line. The population-average exposure to stressfully warm and attributable temperatures for people living on seven land masses are plotted as thin lines. Note that for all time series, the 2023 value is the total over the last 12 months. B. The spatial distribution of days above the 83rd percentile November 2022-October 2023. C. The distribution of days above the threshold that also have ChIP>=1. See Figure S3 for cold temperatures.

Table 1. The cities with the 20 longest streaks of temperatures above their local 99th percentile level. The number of days, starting date (day/month), and mean ChIP over the streak are listed for each city. We also calculate the ChIP for the multi-day average temperature and express this as the equivalent likelihood ratio. The largest value in each column is indicated in bold. Statistics for the full set of 700 cities is available in the supplementary material.

City	Country	Longest Streak	Starting Date	Mean ChIP	Multi-Day ChIP	Ratio
Houston	United States	***22***	7/31	3.4	3.2	9.1
Tangerang	Indonesia	17	10/7	3.5	4.1	17.0
New Orleans	United States	17	7/30	3.2	4.1	17.1
Jakarta	Indonesia	17	10/7	3.5	4.1	17.0
Austin	United States	16	7/31	3.2	6.3	78.4
Qujing	China	16	5/20	3.0	5.9	60.8
Bekasi	Indonesia	15	10/7	3.8	5.3	40.0
Guadalajara	Mexico	15	6/12	3.6	4.9	29.7
Zapopan	Mexico	15	6/12	3.5	4.7	26.7
San Antonio	United States	15	8/4	3.5	3.8	13.5
Dallas	United States	14	8/1	2.9	5.9	58.3
Manaus	Brazil	14	9/30	3.5	4.6	24.4
Havana	Cuba	12	8/3	***4.0***	4.4	20.4
Monterrey	Mexico	12	6/13	3.9	5.2	36.8
Santo Domingo	Dominican Republic	12	9/25	3.9	5.1	35.2
Phoenix	United States	12	7/12	3.6	4.4	21.3
Tunis	Tunisia	11	7/15	3.9	5.4	43.4
Palembang	Indonesia	11	9/28	3.6	6.0	65.5
Visakhapatnam	India	11	6/7	1.3	2.3	4.9
Miami	United States	10	8/6	3.8	***7.3***	***157.5***

Supporting Information for

High-resolution attribution of the daily exposure of people and ecosystems to climate-driven heat

Supporting Text

ChIP and Information Theory

Here we develop a metric based on information theory that can quantify everyday experiences with climate change.

Consider an event $T(x,y,t)$ in our current climate. T could be any event, but for this study, we consider daily observations of air temperature. Suppose we have an observer who is familiar with the statistics of temperature at their location. We quantify their familiarity using a probability density function, $P_{modern}(T)$. For temperature, P_{modern} will often be close to normally distributed. The observer is not surprised by temperatures that fall near the center of the distribution, but they are surprised by temperatures in the tails.

Information theory defines surprise as the negative log of the probability of the event, i.e.:

$$S_{modern}(T) = -\log_2 P_{modern}(T). \quad (1)$$

S_{modern} is the amount of information the observer acquires about their modern climate by observing the event.

We then introduce a second observer, one who is familiar with the statistics of temperature in the counterfactual climate with no human-caused climate change. This observer will have their own expectations represented by $P_{counter}$ and their own level of surprise, $S_{counter}$. We contrast how experiencing a particular temperature impacts the two observers' understanding of the world by taking the difference between their levels of surprise. This is the definition of the change in information due to perspective (ChIP):

$$ChIP(T) = S_{counter}(T) - S_{modern}(T) . \quad (2)$$

This equation tells us how much more surprising the temperature is in the counterfactual climate compared with the modern climate. For example, suppose an event has $S_{modern} = 1$, indicating a that it is surprising to the modern observer. This event would likely be even more surprising to the counterfactual observer (for example, $S_{counter} = 3$). The ChIP value for this event would be 2. The ChIP is how much more information the counterfactual observer gains by observing an event in our climate-changed world. For the modern observer, ChIP is the information advantage they have due to their understanding of climate change.

Calculating ChIP

The main text contains a high-level description of our daily attribution methodology. Additional details are provided below.

Scale Factors

Our implementation of the G22 empirical approaches begin by creating a time series of the qth quantile of the temperature distribution at a given location for a 31 day period centered on day = d. For each period d, we used linear regression to compute

$$T_d(yr, x, q) = \beta(d, x, q)\, \mathrm{GMT}(yr) + c \quad (S1)$$

where GMT(yr) is the 3-year smoothed HadCRUT5 global mean temperature centered on year=yr, and $T_d(yr, x, q)$ is the temperature of the qth quantile for the period. We fit (S1) for the period 1950-2021 using 21 evenly-spaced values of q between 0.01 and 0.99, and we did this for Tmin, Tmax, and Tavg.

The coefficient $\beta(d, x, q)$ is called the "scale factor", and it is the key output of this process. The scale factor describes how we expect the temperature at location x to change in response to a change in GMT.

Empirical Skew Normal Distributions

The most significant change between our approach and G22 is that we used skew normal distributions to represent the likelihood of daily temperatures. The skew normal distribution is described by the location parameter (analogous to a median), the scale parameter (analogous to the variance), and the shape parameter that defines the level of skewness.

To compute SN_{GMT}, the skew-normal distribution representing a climate with a specific global mean temperature, we first assemble daily data from the reference period (1991-2020) for the 31 day period surrounding the target period. Next, we binned the data into intervals defined by the quantiles. We then used the scale factors from (S1) to shift the data in each bin from the reference climate to the climate of GMT:

$$T_{GMT}(x, q) = T_{ref}(x, q) + \beta(d, x, q)\ (\text{GMT} - \text{GMT}_{ref}) \quad \text{(S2)}$$

where GMT_{ref} is the mean GMT over the 1991-2020 reference period. Finally, we use SciPy's skewnorm.fit function to find the parameters that produce a skew normal continuous distribution function that most closely approximates T_{GMT}. We computed SN_{GMT} for GMT = 0.0° (the counterfactual climate) and for GMT between 0.2° and 1.3° at steps of 0.1°.

We also calculated SN_{ref} the skew-normal distribution fit to the distribution of daily data for the 1991-2020 reference period. This distribution gives us a second way of estimating the modern and counterfactual likelihood by adjusting the temperature by $-\beta(d, x, 0.5)(\text{GMT} - \text{GMT}_{ref})$. These distributions assume that climate change only changes the median temperature at a location, not the variance or skewness of the distribution.

Empirical Estimates of ChIP(T)

For the temperature T (Tmin, Tmax, and Tavg) at every ERA5 location and day, we computed two versions of the change in information due to perspective, ChIP(T). The ChIP requires estimates of how surprising T is in the modern and counterfactual climates. We calculated $\text{ChIP}_{median}(T)$ using SN_{ref}, adjusting the T using β (Table S1). We calculated $\text{ChIP}_{quantile}(T)$ using the climate-specific skew normal SN_G, where G is the desired GMT rounded to the nearest 0.1°. All values of ChIP were restricted to the range [-4, 4].

For our attribution assessments, we removed the year-to-year variability from the global mean temperature time series to focus on the long-term trend in the climate. We used the linear trend based on the prior 30 years to estimate GMT:

$$\text{GMT}(yr) = \gamma_{30}(yr)\ \ yr + c_{30},(yr) \quad \text{(S3)}$$

where γ_{30} and c_{30} are the coefficients from the linear regression of GMT against year over the 30 preceding years (e.g. 1992-2021 for yr=2022). The values estimated using the 30 year regression are strongly related to those using a centered 11 year mean (R^2=0.97, p<0.01), but can be applied for the most recent years..

Model-based method

The empirical methods use the relationship between local and global mean temperatures to construct the counterfactual distributions. Climate models provide a more direct estimate of the influence of anthropogenic greenhouse gas emissions on local conditions.

We used 24 models from CMIP6 that had historical runs, forced projections (SSP3-7.0 if available, SSP5-8.5 in some cases), and pre-industrial control runs (Table S2). For each model, we used Tmax = tasmax and Tmin = tasmin and constructed Tavg. We concatenated the historical and projections for each model to create a single "forced" simulation for each model.

We used the xESMF (1) regridder to regrid each model to a common 1.5°-by-1.5° grid. For the 16 models that had coarser resolution, we used bi-linear interpolation (xesmf's "bi-linear" method). For the 8 models that had finer resolution, we used the xesmf "conservative" method.

As in G22 we bias-adjust the output of each individual climate model using (2). We used the same 1991-2020 ERA5 climatology (regridded to 1.5°) as in our empirical method as the reference data for the debiasing. The debiasing trained by the relationship between the reference climate and the forced simulations was likewise applied to debias each paired pre-industrial control simulation.

For each model, we identified the first year when its representation of GMT (smoothed using an 11year running mean) was greater than or equal to each of the 12 GMT values used in the empirical methods. We selected the 31 year period centered around the year to assess the climate corresponding to that GMT. For each of the 24 periods in the year, as with the empirical method, we extract the 31 day period centered around the target day. We then fit skew normal distributions to the Tmin, Tmax, and Tavg data. We also extract the same range of days from the last 31 years of the pre-industrial control run and fit a counterfactual skew normal distribution.

For each model M, we can calculate $\text{ChIP}_M(T)$ as

$$\text{ChIP}_M(T) = - \log_2(\text{SN}_{M,0}\,(T)) + \log_2(\text{SN}_{M,G}\,(T)) \tag{S3}$$

where $\text{SN}_{M,0}$ is the skew normal distribution for the control run and $\text{SN}_{M,G}$ is the distribution from the forced run corresponding to GMT=G. Each estimate was restricted to the same [-4, 4] range.

Combining ChIP Estimates

For a given day and temperature variable, we have 26 estimates of the change in information: the two empirical estimates (ChIP_{median} and $\text{ChIP}_{quantile}$) and the 24 model estimates (ChIP_M). We combined these into a single estimate:

$$\text{ChIP}(T) = 0.5\ (\text{ChIP}_{empirical}(T) + \ \text{ChIP}_{model}(T)) \tag{S4}$$

where $\text{ChIP}_{empirical}$ is the average of the two empirical methods and ChIP_{model} is the average of the 24 models.

Properties of ChIP

While it is not strictly necessary to specify the base in the definition of ChIP (i.e. equation 1), we use base-2. This technically means that S_{modern} is in units of bits of information, but these bits are different than the discrete 0/1 used in computers.

A key property of the ChIP is that sums and averages are meaningful. For example, suppose the temperature on day one has an occurrence ratio of 2 (twice as likely because of climate change), and the next day has an occurrence ratio of 1/2 (half as likely). The average of these two ratios is 1.25, which would imply elevated probabilities due to climate change. In contrast, the ChIP for these two days are 1 and -1. The average of these two days gives ChIP = 0 meaning that together, there is no new information of climate change from these two days.

Assuming normal distributions, it is straightforward to show that the ChIP of an n-day average temperature is proportional to the average of the n daily ChIP values:

$$\text{ChIP}(\frac{1}{n}\sum_{d=1}^{n} T_d) = \frac{\sigma_d^2}{\sigma_n^2}\frac{1}{n}\sum_{d=1}^{n}\text{ChIP}(T_d) \tag{S5}$$

where σ_d is the standard deviation of daily observations and σ_n is the standard deviation of n-day averages. While (S5) does not account for autocorrelation, simulation experiments show that it gives a reliable estimate for multi-day ChIP values, even if the underlying data are strongly autocorrelated.

Uncertainty of ChIP

To compute a confidence interval around a ChIP estimate, we use the confidence interval of the scale factor (β) from the regression of local temperature against GMT. By using the lower and upper bounds in S3, we get the confidence interval of ChIP from the empirical method, and translate it into a standard error (SE_e) assuming the ChIP is close to normally distributed. We then calculate the standard error of the ChIP estimates across the climate models (SE_m). The two estimates of the standard errors are then combined using the formula

$$SE_{average} = 0.5\ (SE_e^2+SE_m^2)^{1/2} \quad \text{(S6)}$$

For the maximum exposure date, the area-weighted mean standard error is 0.29. There is higher uncertainty in polar regions (Figure S4).

Note that S6 does not take into account the range limits we placed on ChIP. This means that our area- and population-weighted means are underestimates of the true ChIP, and that for high values values of ChIP, S6 will overestimate the error.

National Summaries

Table S2 lists the socio-economic or geographic classification of each country, consistent with (15). For each country, we include the population-weighted average temperature anomaly and ChIP for the maximum exposure day (August 21, 2023)

Extreme Heat in Global Cities

We identified 700 cities with a population of more than 1 million people. We associated each city with its nearest ERA5 grid cell. Based on 1991-2020, we calculated each city's 99th percentile temperature. Then, for the period November 2022-October 2023, we identified days that exceeded this threshold (Table S3). We searched for streaks of five or more consecutive days above this threshold. For any city with a streak, we calculate the average ChIP over the streak. For the 20 cities with the longest streaks (Table 1 in the main manuscript), we used the daily ChIP data from 1991-2020 to estimate the variance over the period of the streak and the year-to-year variance of n-day averages. We then applied (S5) to calculate the ChIP for the entire streak.

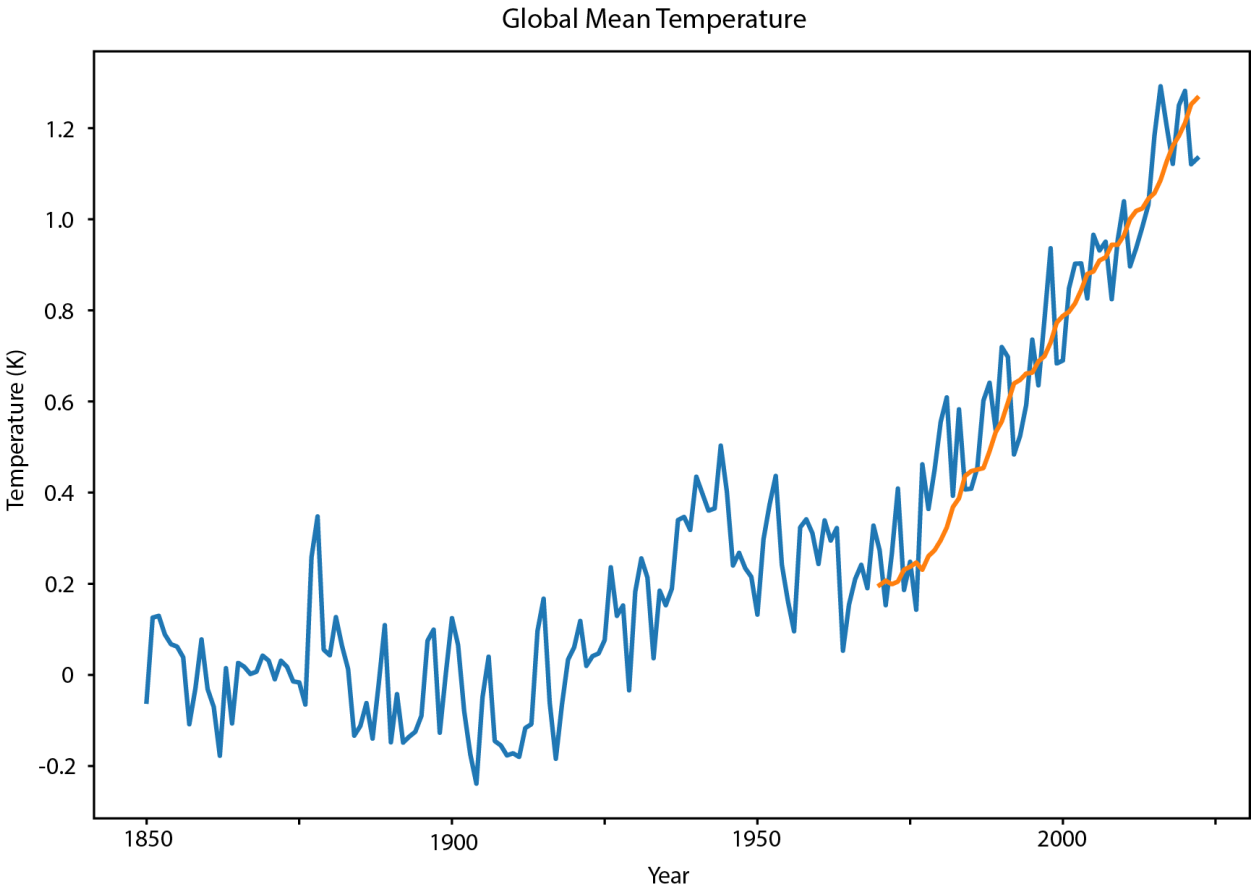

Figure S1. HadCRUT5 global mean temperature referenced to the mean of the period 1850 to1899. The smoothed values represented by the orange line were used to define the climate of a given year for the attribution analysis. It is the linear regression of the prior 30 years projected into the specified year.

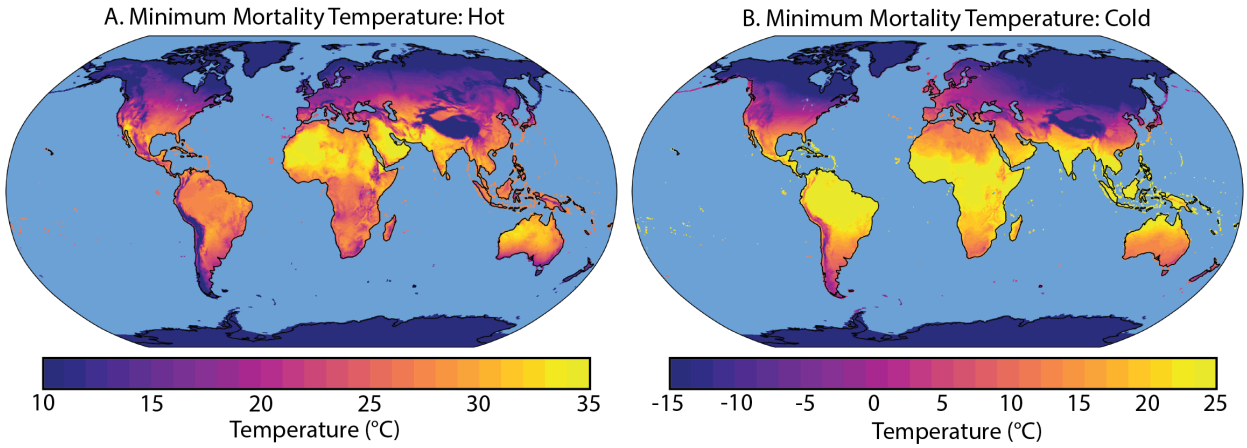

Figure S2. Reference temperatures for the health exposure analysis. A. Minimum mortality temperature defined as the 83rd percentile of daily Tavg for 1986-2005. B. The 17th percentile temperature used to define hazardous cold temperatures. Note that the panels use different color scales.

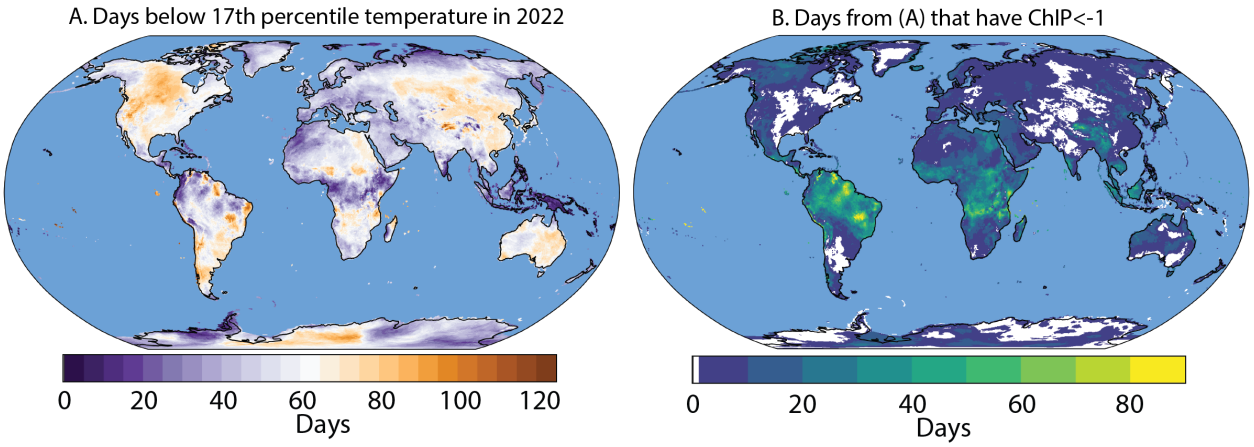

Figure S3. Exposure to stressful cold temperatures. Same as Figure 4 B-C in the main text but for cold days. A. The spatial distribution of days below the 17th percentile in 2022. B. The distribution of days below the threshold that also have ChIP<=-1. Note that this is not strictly analogous to Figure 4C in terms of its interpretability as an indicator of attribution to climate change.

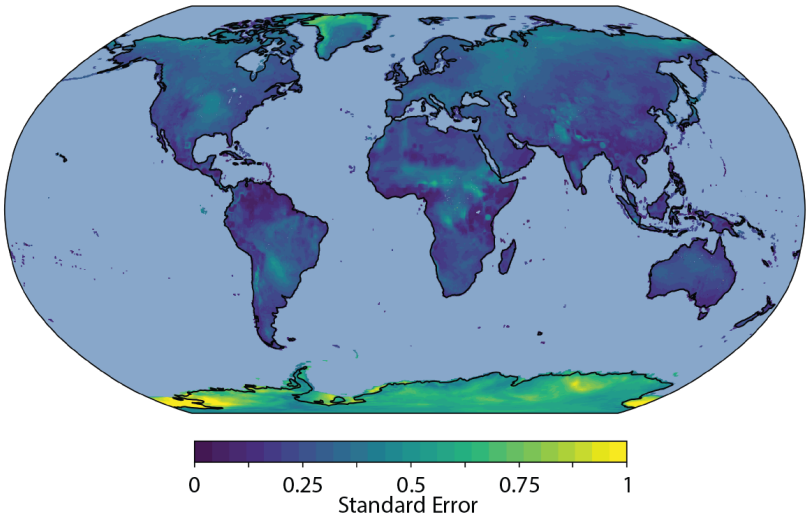

Figure S4. Standard error of Tavg for August 22, 2023.

Table S1. Components to calculate ChIP(T) for the two empirical methods.

	Global Mean Temperature	**ChIP$_{median}$ = $S_{counter}$ - S_{modern}**	**ChIP$_{quantile}$ = $S_{counter}$ - S_{modern}**
$S_{counter}(T)$	0°	$-\log_2(SN_{ref}\,(T-\beta\,(0-GMT_{ref}))$	$-\log_2(SN_0\,(T))$
$S_{modern}(T)$	GMT	$-\log_2(SN_{ref}\,(T-\beta\,(GMT-GMT_{ref}))$	$-\log_2(SN_G\,(T))$, G = GMT rounded to 0.1°

Table S2. Population-weighted average ChIP and temperature anomaly values for 186 countries on August 21, 2023. Each country was categorized into the same regions and human development index categories used by the Lancet Countdown (15). For each variable (Tavg, Tmax, and Tmin), we report the per-capita average ChIP

Table S2 has been uploaded as a Supplementary Dataset in CSV format

Table S3. Extreme temperatures in 700 cities during November 2022-October 2023. For each city, we report the number of days above the 99th percentile temperature. If a city had a continuous streak of five or more days of extreme temperatures, we reported the length of the longest streak and the mean ChIP over the streak.

Table S3 has been uploaded as a Supplementary Dataset in CSV format

Supplementary References

1. J. Zhuang, R. Dussin, A. Jüling, S. Rasp (2020) xESMF: v0.3.0.
2. S. Lange, Trend-preserving bias adjustment and statistical downscaling with ISIMIP3BASD (v1. 0). Geoscientific Model Development 12, 3055-3070 (2019).